International Journal of Hydrogen Energy 66 (2024) 48–54

Contents lists available at ScienceDirect

International Journal of Hydrogen Energy

journal homepage: www.elsevier.com/locate/he

Short Communication

A tubular electrochemical hydrogen compressor

Wibke Zängler [a], Mojtaba Mohseni [a], Robert Keller [a], Matthias Wessling [a,b,*]

[a] RWTH Aachen University, Chemical Process Engineering, Forckenbeckstr. 51, Aachen, 52074, Germany
[b] DWI - Leibniz Institute for Interactive Materials, Forckenbeckstr. 50, Aachen, 52074, Germany

ARTICLE INFO

Keywords:
Electrochemical hydrogen compression
Tubular electrochemical reactor
Tubular membrane electrode assembly
Electrochemical cell design
Hydrogen

ABSTRACT

Electrochemical hydrogen compression is a promising alternative to conventional mechanical compression due to low maintenance costs and high one-stage compression ratios. The typically employed planar systems, however, are intrinsically difficult to operate in high differential pressure environments. Tubular systems are inherently advantageous for high differential pressure systems but require innovative membrane electrode assembly development. This study unveils the first tubular EHC featuring a membrane electrode assembly supported by a stainless steel 3D-printed porous anode. The membrane electrode assembly for gas-phase electrochemistry is produced by spray coating the porous anode with Pt/C as the catalyst and joining the anode with a tubular catalyst-coated membrane. Electrochemical characterization demonstrates the functionality of the tubular EHC at current densities up to 60 $mAcm^{-2}$ with a cell potential of 200 mV under non-pressurized conditions. Moreover, a pressure difference of 2 bar is achieved at 60 $mAcm^{-2}$ within the first 60 min in continuous mode. By demonstrating the proof-of-principle for the first tubular EHC, this work paves the way for new research avenues in electrochemical process engineering, offering a broad spectrum of applications, from enhancing EHC technologies to advancing electrochemical CO_2 reduction.

1. Introduction

Hydrogen is envisioned as the central energy vector in a defossilized economy [1,2]. By increasing the contribution of renewable energies, the role of hydrogen as chemical energy storage becomes increasingly important. Nevertheless, due to the low volumetric energy density of hydrogen, compression is of paramount importance in hydrogen processing [3–7]. Currently, mechanical compressors are used for hydrogen compression. These are usually positive replacement devices, e.g., membrane and piston compressors [5]. Mechanical compression is a mature technology which offers single-stage compression ratios up to seven. However, it entails limitations such as vibration, moderate efficiency (45% [5]) due to the isentropic compression principle, and high maintenance costs due to mechanical wear [8–10].

Alternatively, electrochemical hydrogen compression (EHC) is an emerging technology to overcome the challenges of its mechanical counterpart because no moving parts are incorporated in the device. Additionally, theoretically unlimited compression ratios and efficient compression in small systems can be achieved, offering enhanced flexibility [6,11,12]. In addition, less theoretical compression work is required due to the isothermal compression [13].

In EHC, low-pressure hydrogen is supplied to the anode of an electrochemical cell, where it oxidizes to protons and electrons (Eq. (1)). The applied electrical driving force causes the protons to migrate through a proton exchange membrane (PEM) toward the cathode while the electrons flow through an external electrical circuit. At the cathode, the protons are reduced to hydrogen (Eq. (2)).

$$H_{2,\ \text{low p}} \longrightarrow 2H^+ + 2e^- \tag{1}$$

$$2H^+ + 2e^- \longrightarrow H_{2,\ \text{high p}} \tag{2}$$

Through the applied electrical driving force, the pressure of hydrogen is increased towards the cathode side. The potential compression relationship is governed by the Nernst equation (Eq. (3)) [14,15]:

$$E = \frac{RT}{2F} \ln \frac{p_c}{p_a} \tag{3}$$

with R the ideal gas constant, T the process temperature, F the Faraday constant, and p_c, p_a the cathode and anode hydrogen partial pressure.

Planar EHC stacks are comprised of membrane electrode assemblies: Either the anode and cathode catalyst layers (mainly platinum and its alloys) are deposited on gas diffusion layers (including a microporous layer, mainly carbon materials), which are pressed onto a proton exchange membrane (PEM, mainly per-/polyflourosulfonic acid (PFSA)-based). Alternatively, catalyst-coated membranes, where the catalyst is directly applied onto the PEM, can be sandwiched between gas diffusion layers. Additionally, bipolar plates containing gas flow

* Correspondence to: RWTH Aachen University, Aachener Verfahrenstechnik - Chemical Process Engineering, Forckenbeckstr. 51, 52074 Aachen, Germany.
E-mail address: manuscripts.cvt@avt.rwth-aachen.de (M. Wessling).

https://doi.org/10.1016/j.ijhydene.2024.03.355
Received 8 February 2024; Received in revised form 25 March 2024; Accepted 28 March 2024
Available online 11 April 2024

fields, gaskets, and end plates with bolts to tighten the cell or cell stack are needed to assemble an EHC [11,16,17].

The main challenges in EHC are membrane and catalyst materials, water mass transport to humidify the PEM, sealing, and cost [16,18–20]. State-of-the-art catalysts in EHC are platinum group metals, which are costly and are susceptible to catalyst poisoning in media containing impurities, e.g., by CO [21]. Most ion exchange membrane materials used in EHC must be sufficiently humidified to ensure ion conductivity, which is challenging to maintain in a process with a gaseous reactant and product such as EHC [19]. Moreover, the back-permeation of hydrogen through the ion exchange membrane is limiting the process efficiency of EHC. Additionally, sealing concepts for high-pressure applications are challenging [22].

While there have been some studies on catalyst [23,24] and membrane [25–27] development for EHC, research on process aspects e.g. cell geometry, flow field, and gas diffusion layer design, sealings, and reactor designs has been limited [28,29].

Tubular cell designs offer advantages in sealing length, surface-to-volume ratio, and mass transport [30–33]. Additionally, tubular systems are intrinsically well-suited for differential pressure applications such as EHC. Additionally, uniform pressure distribution on the cell compared to planar ones can lead to lower ohmic losses and, consequently, less stress on the membrane and mechanical support for the PEM in tubular cells [18,34].

Despite these advantages, tubular cell concepts, especially including membrane electrode assemblies, have been sparsely realized [30,35,36]. Laube et al. [30] developed a tubular membrane electrode assembly for PEM-electrolyzers, which can be fabricated through cost-effective and in-line co-extrusion. Recently, they achieved $450\,mA\,cm^{-2}$ at $2\,V$ in their tubular PEM water-electrolyzer [37]. Dong et al. [36] developed a solid electrolyte tubular cell for CO_2 electroreduction using a SN-Cu hollow fiber electrode, reporting a cell potential of $-1.4\,V$ at $0.11\,mA\,cm^{-2}$ for acetaldehyde and acetone production.

However, in both studies, liquid electrolytes were employed. To date, no tubular concepts for all gas phase electrochemistry, e.g., EHC, have been presented. These pose specific challenges as mass transport to and from the catalytic site.

This work introduces the first all-tubular EHC with a membrane electrode assembly comprising a 3D-printed anode and a catalyst-coated membrane. The EHC's electrochemical performance was examined in a tubular module via linear sweep, multi-chronopotentiometry, and electrochemical impedance spectroscopy. The compression performance was tested in short-term stability experiments.

2. Material and methods

2.1. Materials

Pt/C nanoparticles 40% Pt on carbon black and Fumion 1005, 5% suspension in n-propanol were purchased from Quintech. NAFION® tubes with 2.18 mm inner diameter and $305\,\mu m$ membrane thickness were supplied by Permapure.

2.2. Anode fabrication

The porous tubular anodes of $8\,cm$ length, $3.3\,mm$ outer diameter, and $1\,mm$ wall thickness were produced by metal selective laser melting (SLM) using a selective laser fusion printer (Sisma MySint100 PM), enabling tunable pore size and porosity. Stainless steel powder 1.4404 (AISI 316L, particle size <60 μm) was employed as substrate. The anode was produced with a radial pore pattern, which was achieved by scan line patterning developed by Limper et al. [38]. The SEM image in Fig. 1 shows the radial pore pattern of the shell side and cross section of the tubular porous support. The pore size distribution of the herein used anode is presented in Figure S1. The pore size distribution and morphology of the anode were measured via gas–liquid porosimetry (POROLOX 1000, Porometer NV) and scanning electron microscopy (SEM) (TM3030plus, Hitachi), respectively.

2.3. Catalyst-coated membrane fabrication and MEA assembly

The catalyst ink was prepared by sonicating a mixture of $14\,mg$ Pt/C nanoparticles, $2.3\,mL$ isopropanol, $100\,\mu L$ Fumion 1005 suspension for 30 min (amounts for one 8 cm tube). First, the ink was airbrushed on the tubular anode via manual spray coating (Harder & Steinbeck, Evolution Infinity). The theoretical catalyst loading of the anode and cathode is $0.7\,mg\,cm^{-2}$. The catalyst layer was dried for two hours at a vacuum of $50\,mbar$ and a temperature $80\,°C$. Subsequently, the NAFION® tube was soaked in 80% methanol in DI-water for at least twelve hours, then slid on the tubular anode and dried at ambient conditions for 24 h, which led to a firm shrinkage of the membrane on the anode. Afterward, the cathode catalyst layer was sprayed on the outer surface of the membrane using the same parameters as for the anode.

2.4. Tubular EHC assembly

The tubular anode was contacted via a silver-coated copper wire as the current collector by ultrasonic soldering (MBR electronics). The cathode of the tubular membrane electrode assembly was contacted by titanium felt (Bekaert, $20\,\mu m$ fiber diameter, $400\,gm^{-2}$ weight, nominal porosity of 50%, shown in Figure S2) and a stainless steel clamp (3D-printed), as shown in Fig. 1. Three bolts ensure the tightness of the clamp for electrical contacting.

The membrane electrode assembly was potted into polyethylene tubing using two component epoxy resin (UHU Plus Epoxy Ultra Quick) and then installed into the reactor. All experiments were conducted in an in-house fabricated tubular reactor, depicted in Fig. 2.

2.5. Electrochemical experiments and analytics

All experiments were executed in a two electrode set-up and at room temperature. Mass flow controllers (Series 358, Analyt MTC) were used to control the gas supply to the cell. The relative humidity was monitored by a humidity sensor (UFT75-ST1, MELTEC). The back pressure on the cathode side was regulated by a check valve (Spring loaded back pressure regulator, Swagelok), if required, and monitored (A-10, WIKA).

Before supplying hydrogen, the anode and cathode compartments of the reactor were flushed with nitrogen for safety reasons. For preconditioning, humidified hydrogen (100% RH) with a flow rate of $50\,N\,mL\,min^{-1}$ was fed to the anode, starting 20 min in advance of each experiment to ensure saturation of the compartment with hydrogen.

Electrochemical experiments were conducted by a biologic VSP potentiostat with a booster (VMP3B-20) and impedance module. Polarization curves were obtained by multi-chronopotentiometry experiments with a step duration of 40 min. The mean value of the last five minutes of the current step is displayed in the polarization curve. All electrochemical impedance measurements were performed at OCV with $10\,mV$ perturbation and six points per decade. Electrochemical impedance spectra were measured from $10\,kHz$ to $1\,kHz$ before an experimental series and from $10\,kHz$ to $10\,Hz$ for all other impedance measurements. Linear sweep voltammetry (LSV) measurements were performed with $500\,mV\,s^{-1}$ scan rate. The ohmic resistance for the LSV was determined at $5\,kHz$, and 85% iR-compensation was considered. Unless otherwise mentioned, all data is presented as the mean value of duplicate experiments, with the standard deviation as the error bar.

3. Results and discussion

Design concept

Electrical contacting is a significant challenge for small, tubular designs. For adequate contact, sufficient pressure must be applied on the membrane electrode assembly, requiring high mechanical stability of the centered anode as it bears the applied force. The herein employed

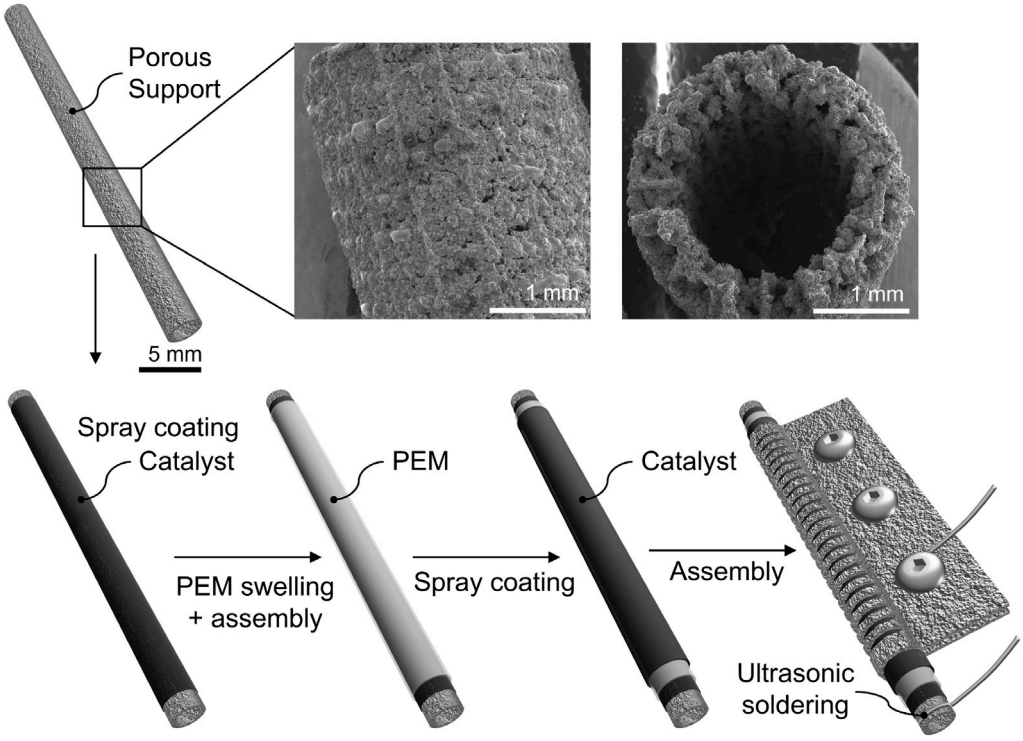

Fig. 1. Assembly of tubular electrochemical hydrogen compressors. Porous support prepared by 3D-printing. SEM image of porous support shell side and cross section. Anode and cathode catalyst layers are prepared by manual spray coating Pt/C catalyst ink. Anode and cathode catalysts are separated by a commercial NAFION® tube. The cathode is contacted via a stainless steel clamp.

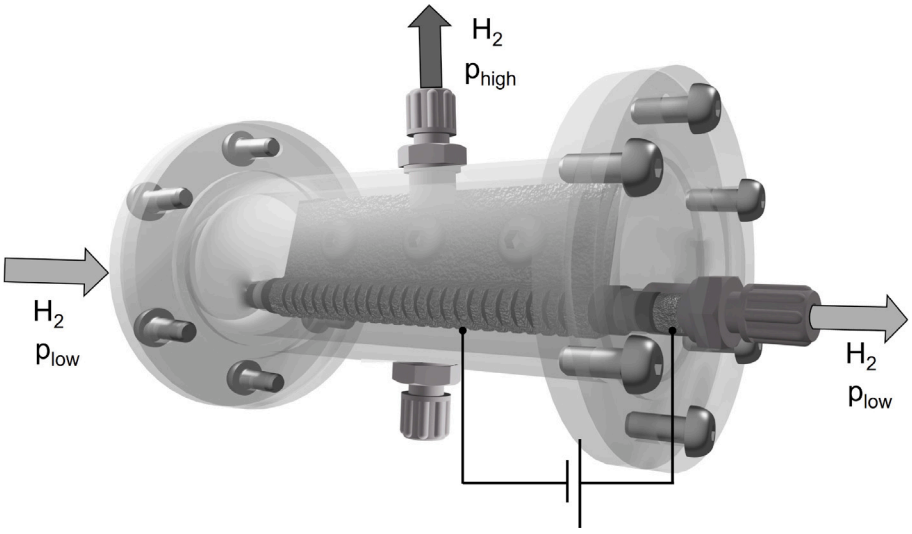

Fig. 2. Reactor for the operation of tubular EHC.

3D-printed metal anode with tunable porosity provides sufficient mechanical stability. The tailor-made clamping device also ensures a uniform pressure distribution from the cathode to the membrane and anode. Additionally, the design facilitates self-reinforcement, as the pressurized side of the cell is the cathode side. A pressure gradient between the cathode and anode develops upon electrochemical hydrogen compression, pressing the MEA onto the rigid anode support.

Electrochemical characterization

The tubular EHC was characterized electrochemically by linear sweep voltammetry, multi-chronopotentiometry, and electrochemical impedance spectroscopy. Fig. 3(a) shows the iR-corrected and non-corrected polarization curve of the tubular EHC as well as the results from the multi-chronopotentiometry. Linear behavior of the polarization curves is observed until 60 mA cm^{-2}, followed by an exponential increase at higher current densities. The current–voltage behavior is validated by the results from the multi-chronopotentiometry (square symbols). The limiting current density under non-pressurized operation conditions reached approximately 90 mA cm^{-2}. Fig. 3(b) presents the Nyquist plot of electrochemical impedance spectra recorded between multi-chronopotentiometry experiments. The current and voltage response of the consecutive runs between the impedance spectra is presented in Figure S3. The high frequency resistance of the cell ranged between 2 to 2.75 Ω cm^2 in electrochemical impedance measurements (Fig. 3(b)).

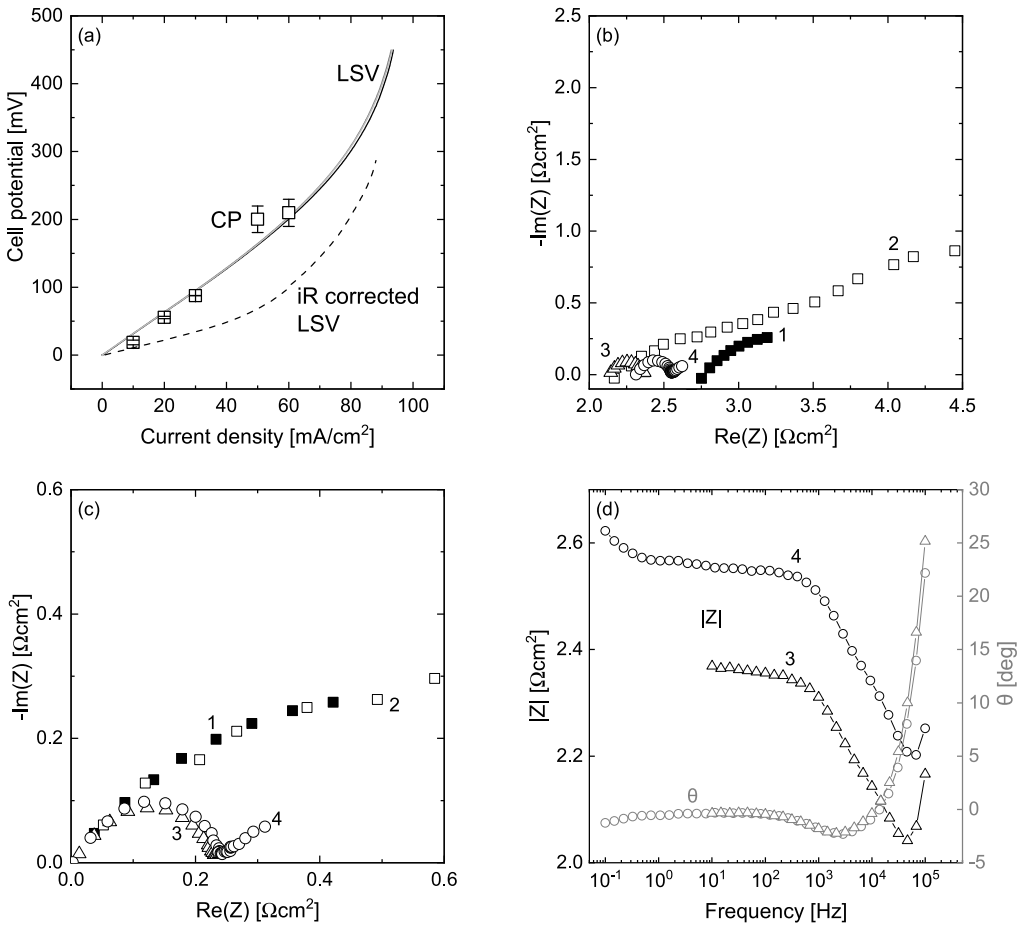

Fig. 3. (a) Steady-state current–voltage behavior of tubular EHC recorded by current steps (40 min, circles) and polarization behavior recorded by linear sweep voltammetry (solid lines) and iR corrected linear sweep (dashed line), 50 ml/min H_2, 100% relative humidity in the feed gas; (b) Nyquist plot of impedance spectra consecutively recorded between multi-chronopotentiometry experiments, 1: after preconditioning of the cell, 2: after 2.5 h at 10 mA cm^{-2}, 3: after 2.5 h at 40 mA cm^{-2}, 4: after 2.5 h at 60 mA cm^{-2}; (c) zoom in on high frequencies of (b) all spectra shifted to zero ohmic resistance; (d) Bode diagram of measurement 3 and 4.

In comparison, studies on planar EHCs have reported limiting current densities ranging from 0.5 to 3.5 A cm^{-2} at room temperature, which is significantly higher than achieved in this work [17,39]. For instance, Zou et al. achieved 3.5 A cm^{-2} with similar catalyst loading as in this study but with a significantly thinner ion exchange membrane of 15 µm compared to 300 µm in this work. The iR-corrected linear sweep (Fig. 3(a)) demonstrates cell potentials comparable to those in the literature and emphasizes major ohmic loss contributions to overall cell performance. For example, at a current density of 50 mA cm^{-2}, the potential declines from 150 mV to 50 mV after iR correction. However, it should be noted that this work introduces the first tubular EHC, and the potential for optimization is thus not yet tapped.

Possible reasons for the limited electrochemical performance of the tubular EHC, especially at current densities above 60 mA cm^{-2}, might be drying out of the proton exchange membrane, condensation of water in the porous support or on the electrodes, and corrosion of the stainless steel anode support. At higher current densities, more water is needed to maintain a sufficient wetting degree of the proton exchange membrane. Thus, non-ideal humidification of the proton exchange membrane, due to mass-transport limitations in the porous transport layer of the anode, could lead to an increase of the cell potential at higher current densities [10,40].

This hypothesis can be underlined by the impedance data (Fig. 3(b)). After preconditioning (Fig. 3(b), plot 1), the ohmic resistance of the cell is 2.75 Ω cm^2. After 2.5 h chronopotentiometry at 10 mA cm^{-2}, the ohmic resistance drops to 2.18 Ω cm^2 (plot 2), but the Nyquist plot qualitatively remains similar to the initial spectrum. After 2.5 h chronopotentiometry at 40 mA cm^{-2} (plot 3), the first semicircle in the Nyquist plot is significantly smaller. The spectrum's shape changes over the whole frequency range indicating rehumidification of the membrane [41]. After operation at 60 mA cm^{-2}, the magnitude of the impedance increases (Fig. 3(d)) (plot 4), and the spectrum is shifted to higher resistances (Fig. 3(c)) indicating again the dehumidification of the membrane, also correlating with the increase of potential observed in the linear sweep at current densities above 60 mA cm^{-2} (Fig. 3(a)). After running the cell at 80 mA cm^{-2} (Fig. S3, 5) for 4 min, the spectrum shifts to the initial high-frequency intercept and additionally changes qualitatively, indicating a fundamental change in the electrochemical system such as dehydration of the membrane.

Additionally, water might condense in the hydrophilic porous anode and on the catalyst surface, leading to flooding and resulting in diffusion-limited hydrogen and water vapor transport toward the cathode [42]. In electrochemical impedance analysis, the effect of flooding can be observed in the low-frequency regime. As membrane drying seems to occur simultaneously, changing the impedance spectrum over the whole frequency range, it is difficult to separate the two effects (Fig. 3(b, c)) [41]. Consequently, optimizing the water transport to the EHC membrane is crucial to improve the performance of the herein presented prototype. Moreover, corrosion might occur on the stainless steel anode support structure, leading to increased contact resistance between the anode gas diffusion and anode catalyst layers and, consequently, higher cell potentials [43]. The leaching of iron ions from the stainless steel anode could additionally lead to contamination and severe degradation of the proton exchange membrane, leading to decreased cell performance [44,45].

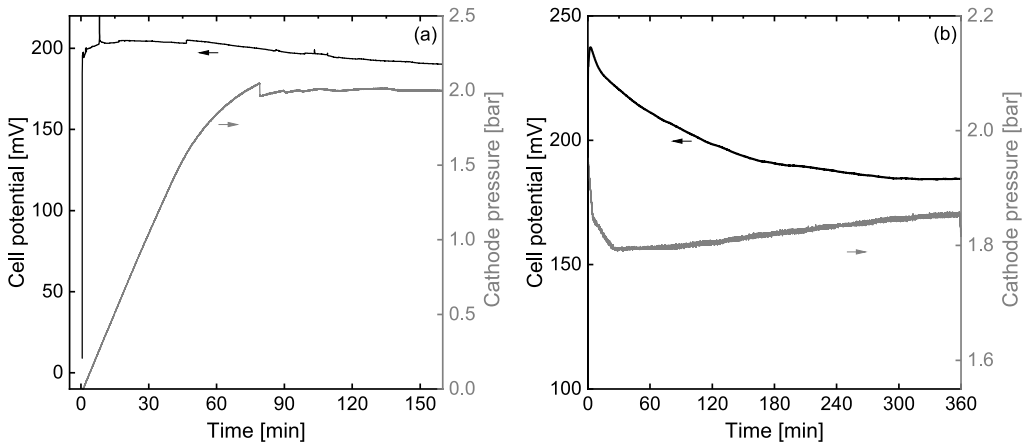

Fig. 4. Cathode pressure (gray) and cell potential (black) of tubular EHC over electrolysis time, 50 mL min^{-1} H_2 feed flow rate equals lambda of 10, 100% relative humidity of the feed gas, (a) 60 mA cm^{-2} constant current, (b) 50 mA cm^{-2} constant current, the three-hours and six-hours experiments were not conducted consecutively.

Hydrogen compression in tubular reactor

The hydrogen compression capability of the tubular EHC was examined at a cathode pressure of 2 bar at a constant current density of 60 mA cm^{-2} for three and at a constant current density of 50 mA cm^{-2} for six hours. It should be noted that the three-hour and six-hour experiments were not conducted consecutively. Fig. 4(a) shows the pressure build-up on the cathode side of the EHC in the initial electrolysis phase. The targeted 2 bar cathode pressure was achieved after 60 min electrolysis. The set pressure was maintained for 100 min at a mean cell potential of 180 mV. In a six-hour experiment, presented in 4(b), the pressure on the cathode side was set to 1.8 bar at the beginning of the experiment. The cell potential decreases from 230 mV to 190 mV during the first 150 min of the experiment. As the cell potential is elevated compared to the 60 min experiment, we hypothesize that the system's preconditioning was insufficient. Thus, in the first 150 min of the experiment, the membrane is hydrated further, and the resistance decreases [40].

This hypothesis is also underlined by the impedance spectra measured before and after the experiment — the high frequency ohmic cell resistance decreases from 3.75 Ω cm^2 to 2.75 Ω cm^2 over the course of the experiment. The cell potential of both pressurized experiments is not significantly different from the non-pressurized experiments, as expected from Eq. (3).

4. Conclusion

This manuscript introduces the first tubular electrochemical hydrogen compressor (EHC) featuring a 3D-printed, stainless-steel porous tubular anode. With this work, an innovative concept is introduced to fabricate tubular membrane electrode assemblies for high differential pressure applications comprising a rigid, 3D-printed anode and a catalyst-coated tubular membrane. Electrochemical testing revealed the tubular MEA's efficacy for gas-phase electrochemistry at current densities up to 60 mA cm^{-2} in continuous mode, reaching a differential pressure of 2 bar across the anode and cathode compartments. Additionally, electrochemical impedance spectroscopy analysis before and after EHC experiments demonstrate the change in electrochemical properties of the EHC, which could be attributed to the membrane drying, flooding caused by water condensation in the porous network of the anode, and contamination due to the undesired leaching of iron ions from the stainless-steel anode. This work spotlights the proof-of-concept for the first tubular EHC, expanding the horizons in the field of EHC, transitioning from planar to tubular modules that promise greater surface-to-volume ratios, superior packing densities and facile high differential pressure operation. The presented module has potential for improvement by considering thinner tubular membranes, inert electrode materials, e.g., titanium, and depositing noble metals for enhanced stability and electrical conductivity, which is under investigation in our group.

CRediT authorship contribution statement

Wibke Zängler: Conceptualization, Data curation, Formal analysis, Investigation, Methodology, Project administration, Supervision, Validation, Visualization, Writing – original draft, Writing – review & editing. **Mojtaba Mohseni:** Conceptualization, Methodology, Supervision, Writing – original draft, Writing – review & editing. **Robert Keller:** Conceptualization, Data curation, Formal analysis, Funding acquisition, Methodology, Project administration, Supervision, Validation, Visualization, Writing – original draft, Writing – review & editing. **Matthias Wessling:** Conceptualization, Funding acquisition, Methodology, Project administration, Resources, Supervision, Visualization, Writing – original draft, Writing – review & editing.

Declaration of competing interest

The authors declare the following financial interests/personal relationships which may be considered as potential competing interests: Matthias Wessling has patent #DE 10 2023 125 255.0 pending to RWTH Aachen University. If there are other authors, they declare that they have no known competing financial interests or personal relationships that could have appeared to influence the work reported in this paper.

Acknowledgments

M. Wessling acknowledges DFG funding through the Gottfried Wilhelm Leibniz Award 2019 [WE 4678/12-1]. R. Keller acknowledges funding by BMBF in the project "ADELE" [grant number 01DR21027]. This work was conducted in part at the Competence Center Industrial Electrochemistry ELECTRA, which is supported by the "European Regional Development Fund" (ERDF) and the Federal State of North Rhine-Westphalia [grant number ERDF 0500077]. The authors thank Alexander Jachertz, Maria Arias Valcarcel, Alexander Bauer, Caroline Schmitz, and Anselm Brodersen for their support.

Appendix A. Supplementary data

Supplementary material related to this article can be found online at https://doi.org/10.1016/j.ijhydene.2024.03.355.

References

[1] Staffell I, Scamman D, Velazquez Abad A, Balcombe P, Dodds PE, Ekins P, Shah N, Ward KR. The role of hydrogen and fuel cells in the global energy system. Energy Environ Sci 2019;12(2):463–91. http://dx.doi.org/10.1039/c8ee01157e.

[2] van der Spek M, Banet C, Bauer C, Gabrielli P, Goldthorpe W, Mazzotti M, Munkejord ST, Røkke NA, Shah N, Sunny N, Sutter D, Trusler JM, Gazzani M. Perspective on the hydrogen economy as a pathway to reach net-zero CO2 emissions in Europe†. Energy Environ Sci 2022;15(3):1034–77. http://dx.doi.org/10.1039/d1ee02118d.

[3] Abe JO, Popoola AP, Ajenifuja E, Popoola OM. Hydrogen energy, economy and storage: Review and recommendation. Int J Hydrog Energy 2019;44(29):15072–86. http://dx.doi.org/10.1016/j.ijhydene.2019.04.068.

[4] Yanxing Z, Maoqiong G, Yuan Z, Xueqiang D, Jun S. Thermodynamics analysis of hydrogen storage based on compressed gaseous hydrogen, liquid hydrogen and cryo-compressed hydrogen. Int J Hydrog Energy 2019;44(31):16833–40. http://dx.doi.org/10.1016/j.ijhydene.2019.04.207.

[5] Sdanghi G, Dillet J, Didierjean S, Fierro V, Maranzana G. Feasibility of hydrogen compression in an electrochemical system: Focus on water transport mechanisms. Fuel Cells 2020;20(3):370–80. http://dx.doi.org/10.1002/fuce.201900068.

[6] Nordio M, Rizzi F, Manzolini G, Mulder M, Raymakers L, Van Sint Annaland M, Gallucci F. Experimental and modelling study of an electrochemical hydrogen compressor. Chem Eng J 2019;369(November 2018):432–42. http://dx.doi.org/10.1016/j.cej.2019.03.106.

[7] Jayakumar A, Madheswaran DK, Kannan A, Sureshvaran U, Sathish J. Can hydrogen be the sustainable fuel for mobility in India in the global context? Int J Hydrogen Energy 2022;47(79):33571–96. http://dx.doi.org/10.1016/j.ijhydene.2022.07.272.

[8] Sdanghi G, Maranzana G, Celzard A, Fierro V. Review of the current technologies and performances of hydrogen compression for stationary and automotive applications. Renew Sustain Energy Rev 2019;102:150–70. http://dx.doi.org/10.1016/j.rser.2018.11.028.

[9] Toghyani S, Baniasadi E, Afshari E, Javani N. Performance analysis and exergoeconomic assessment of a proton exchange membrane compressor for electrochemical hydrogen storage. Int J Hydrog Energy 2020;45(60):34993–5005. http://dx.doi.org/10.1016/j.ijhydene.2020.01.232.

[10] Pivac I, Pavasović AS, Barbir F. Recent advances and perspectives in diagnostics and degradation of electrochemical hydrogen compressors. Int J Hydrog Energy 2024;54:387–96. http://dx.doi.org/10.1016/j.ijhydene.2023.01.281.

[11] Vermaak L, Neomagus HW, Bessarabov DG. Recent advances in membrane-based electrochemical hydrogen separation: A review. Membranes 2021;11(2):127. http://dx.doi.org/10.3390/membranes11020127.

[12] Rhandi M, Trégaro M, Druart F, Deseure J, Chatenet M, Rhandi M, Druart F, Deseure J, Chatenet M, Trégaro M, Druart F, Deseure J, Chatenet M. Electrochemical hydrogen compression and purification versus competing technologies: Part I. Pros and cons. Chinese J Catal 2020;41(5):756–69. http://dx.doi.org/10.1016/S1872-2067(19)63404-2.

[13] Zachert L, Suermann M, Bensmann B, Hanke-Rauschenbach R. Energetic evaluation and optimization of hydrogen generation and compression pathways considering PEM water electrolyzers and electrochemical hydrogen compressors. J Electrochem Soc 2021;168:014504. http://dx.doi.org/10.1149/1945-7111/abcf1a.

[14] Langer SH, Hademan RG. Electrolytic hydrogen purification and recovery of same, U.S. patent 3,475,302. 1969.

[15] Maget HJR. Process for gas purification, U.S. patent 3,489,670. 1970.

[16] Durmus GNB, Colpan CO, Devrim Y. A review on the development of the electrochemical hydrogen compressors. J Power Sources 2021;494:229743. http://dx.doi.org/10.1016/j.jpowsour.2021.229743.

[17] Zou J, Jin Y, Wen Z, Xing S, Han N, Yao K, Zhao Z, Chen M, Fan J, Li H, Wang H. Insights into electrochemical hydrogen compressor operating parameters and membrane electrode assembly degradation mechanisms. J Power Sources 2021;484:229249. http://dx.doi.org/10.1016/j.jpowsour.2020.229249.

[18] Zou J, Han N, Yan J, Feng Q, Wang Y, Zhao Z, Fan J, Zeng L, Li H, Wang H. Electrochemical compression technologies for high-pressure hydrogen: Current status, challenges and perspective. Electrochem Energy Rev 2020;3:690–729. http://dx.doi.org/10.1007/s41918-020-00077-0.

[19] Gong M, Jin C, Na Y. Minimizing area-specific resistance of electrochemical hydrogen compressor under various operating conditions using unsteady 3D single-channel model. Membranes 2023;13(6). http://dx.doi.org/10.3390/membranes13060555.

[20] Chouhan A, Bahar B, Prasad AK. Effect of back-diffusion on the performance of an electrochemical hydrogen compressor. Int J Hydrogen Energy 2020;45(19):10991–9. http://dx.doi.org/10.1016/j.ijhydene.2020.02.048.

[21] Trégaro M, Rhandi M, Druart F, Deseure J, Chatenet M. Electrochemical hydrogen compression and purification versus competing technologies: Part II. Challenges in electrocatalysis. Chinese J Catal 2020;41(5):770–82. http://dx.doi.org/10.1016/S1872-2067(19)63438-8.

[22] Aykut Y, Yurtcan AB. The role of the EHC system in the transition to a sustainable energy future: A review. Int J Hydrogen Energy 2023;48(60):23089–109. http://dx.doi.org/10.1016/j.ijhydene.2023.03.109, The 6th International Hydrogen Technologies Congress (IHTEC-2022).

[23] Wu X, Benziger J, He G. Comparison of Pt and Pd catalysts for hydrogen pump separation from reformate. J Power Sources 2012;218:424–34. http://dx.doi.org/10.1016/j.jpowsour.2012.07.002.

[24] Jackson C, Raymakers LF, Mulder MJ, Kucernak AR. Poison mitigation strategies for the use of impure hydrogen in electrochemical hydrogen pumps and fuel cells. J Power Sources 2020;472:228476. http://dx.doi.org/10.1016/j.jpowsour.2020.228476.

[25] Rico-Zavala A, Gurrola MP, Arriaga LG, Bañuelos JA, Álvarez-Contreras L, Carbone A, Saccà A, Matera FV, Pedicini R, Álvarez A, Ledesma-García J. Synthesis and characterization of composite membranes modified with Halloysite nanotubes and phosphotungstic acid for electrochemical hydrogen pumps. Renew Energy 2018;122:163–72. http://dx.doi.org/10.1016/j.renene.2018.01.054.

[26] Zou J, Huang H, Zaman S, Yao K, Xing S, Chen M, Wang H, Wang M. Enhanced electrochemical hydrogen compression performance with a gradient water-retaining hybrid membrane. Chem Eng J 2023;457:141113. http://dx.doi.org/10.1016/j.cej.2022.141113.

[27] Maxwell DS, Sun Q, Rojas H, Kendrick R, Pavlicek RK, Castro ESD, Aurora A, Mukerjee S. High purity hydrogen separation with HT-PBI based electrochemical pump operation at 120 ° C. J Electrochem Soc 2023;170(034510). http://dx.doi.org/10.1149/1945-7111/acc6f7.

[28] Caponetto R, Privitera E, Mirone G, Matera F. Structural analysis of electrochemical hydrogen compressor end-plates for high-pressure applications. Energies 2022;15(16):5823. http://dx.doi.org/10.3390/en15165823.

[29] Casati C, Longhi P, Zanderighi L, Bianchi F. Some fundamental aspects in electrochemical hydrogen purification/compression. J Power Sources 2008;180(1):103–13. http://dx.doi.org/10.1016/j.jpowsour.2008.01.096.

[30] Laube A, Hofer A, Sánchez Batalla B, Ressel S, Chica A, Fischer S, Weidlich C, Bachmann J, Struckmann T. Tubular membrane electrode assembly for PEM electrolysis. Int J Hydrog Energy 2022;47(36):15943–51. http://dx.doi.org/10.1016/j.ijhydene.2022.03.135.

[31] Coursange JF, Hourri A, Hamelin J. Performance comparison between planar and tubular-shaped PEM fuel cells by three-dimensional numerical simulation. Fuel Cells 2003;3(3):28–36. http://dx.doi.org/10.1002/fuce.200331101.

[32] Mohseni M, Felder D, Percin K, Thönes M, Gassenmeier M, Kupec R, Weidlich C, Linkhorst J, Keller RG, Wessling M. Toward decentralized wastewater treatment: A flow-through module using microtubular gas diffusion electrodes for micropollutants removal. J Hard Mater 2023;458:131987. http://dx.doi.org/10.1016/j.jhazmat.2023.131987.

[33] Weber N, Möntmann M, Wessling M, Keller R. A continuous flow reactor for tubular gas diffusion electrodes. Chem Eng J 2024;486:150031. http://dx.doi.org/10.1016/j.cej.2024.150031.

[34] Ward T, Li X, Faghri A. Performance characteristics of a novel tubular-shaped passive direct methanol fuel cell. J Power Sources 2011;196(15):6264–73. http://dx.doi.org/10.1016/j.jpowsour.2011.04.012.

[35] Rabiee H, Ge L, Hu S, Wang H, Yuan Z. Microtubular electrodes: An emerging electrode configuration for electrocatalysis, bioelectrochemical and water treatment applications. Chem Eng J 2022;450:138476. http://dx.doi.org/10.1016/j.cej.2022.138476.

[36] Dong X, Li G, Chen W, Zhu C, Li T, Song Y, Sun N, Wei W. Gas-phase CO2electroreduction over Sn-Cu hollow fibers. Mater Adv 2021;2(1):241–7. http://dx.doi.org/10.1039/d0ma00851f.

[37] Laube A, Sánchez Batalla B, Weidlich C, Hofer A, Bachmann J, Zallmann S, Körner C, Fischer S, Chica A, Struckmann T. Tubular PEM electrolysis cells with a 3D-printed oxygen electrode and ALD catalyst coating. Int J Hydrog Energy 2023;49:437–48. http://dx.doi.org/10.1016/j.ijhydene.2023.08.084.

[38] Limper A, Weber N, Brodersen A, Keller R, Wessling M, Linkhorst J. Additive manufacturing of composite porosity mixer electrodes. Electrochem Commun 2022;134:107176. http://dx.doi.org/10.1016/j.elecom.2021.107176.

[39] Ströbel R, Oszcipok M, Fasil M, Rohland B, Jörissen L, Garche J. The compression of hydrogen in an electrochemical cell based on a PE fuel cell design. J Power Sources 2002;105(2):208–15. http://dx.doi.org/10.1016/S0378-7753(01)00941-7.

[40] Pineda-Delgado JL, Chávez-Ramirez AU, Gutierrez B CK, Rivas S, Marisela CR, de Jesús Hernández-Cortes R, Menchaca-Rivera JA, Pérez-Robles JF. Effect of relative humidity and temperature on the performance of an electrochemical hydrogen compressor. Appl Energy 2022;311:118617. http://dx.doi.org/10.1016/j.apenergy.2022.118617.

[41] Mérida W, Harrington DA, Le Canut JM, McLean G. Characterisation of proton exchange membrane fuel cell (PEMFC) failures via electrochemical impedance spectroscopy. J Power Sources 2006;161(1):264–74. http://dx.doi.org/10.1016/j.jpowsour.2006.03.067.

[42] Nguyen MT, Grigoriev SA, Kalinnikov AA, Filippov AA, Millet P, Fateev VN. Characterisation of a electrochemical hydrogen pump using electrochemical impedance spectroscopy. J Appl Electrochem 2011;41:1033–42. http://dx.doi.org/10.1007/s10800-011-0341-9.

[43] Miyazawa A, Tada E, Nishikata A. Influence of corrosion of SS316L bipolar plate on PEFC performance. J Power Sources 2013;231:226–33. http://dx.doi.org/10.1016/j.jpowsour.2012.12.088.

[44] Li N, Araya SS, Cui X, Kær SK. The effects of cationic impurities on the performance of proton exchange membrane water electrolyzer. J Power Sources 2020;473:228617. http://dx.doi.org/10.1016/j.jpowsour.2020.228617.

[45] Cheng X, Shi Z, Glass N, Zhang L, Zhang J, Song D, Liu Z-S, Wang H, Shen J. A review of PEM hydrogen fuel cell contamination: Impacts, mechanisms, and mitigation. J Power Sources 2007;165(2):739–56. http://dx.doi.org/10.1016/j.jpowsour.2006.12.012, IBA – HBC 2006.